

Spectral Decomposition of Resting State Electroencephalogram Reveals Unique Theta/Alpha Activity in Schizophrenia

Alexander Nakhnikian¹, Naoya Oribe¹, Shogo Hirano¹, Yuki Fujishima¹, Yoji Hirano¹, Paul Nestor², Grace Francis¹, Margaret Levin³, and Kevin Spencer¹

¹VA Boston Healthcare System

²University of Massachusetts, Boston

³EPhysBio LLC

May 20, 2023

Abstract

Resting state electroencephalographic (EEG) activity in schizophrenia (SZ) is frequently characterized by increased power at slow frequencies, and/or a reduction of peak alpha frequency. Here we investigated the nature of these effects. As most studies to date have been limited by reliance on a priori frequency bands which impose an assumed structure on the data, we performed a data-driven analysis of resting EEG recorded in SZ patients and healthy controls (HC). The sample consisted of 39 chronic SZ and 36 matched HC. The EEG was recorded with a dense electrode array. Power spectral densities were decomposed via Varimax-rotated principal component analysis (PCA) over all participants and for each group separately. Spectral PCA was repeated at the cortical level on cortical current source density computed from standardized low resolution brain electromagnetic tomography. There was a trend for power in the theta/alpha range to be increased in SZ compared to HC, and peak alpha frequency was significantly reduced in SZ. PCA revealed that this frequency shift was due to the presence of a spectral component in the theta/alpha range (6-9 Hz) that was unique to SZ. The source distribution of this component involved mainly prefrontal and parahippocampal areas. Abnormal low frequency resting EEG activity in SZ was accounted for by a unique theta/alpha oscillation. Other reports have described a similar phenomenon suggesting that the neural circuits oscillating in this range are relevant to SZ pathophysiology.

Spectral Decomposition of Resting State Electroencephalogram Reveals Unique Theta/Alpha Activity in Schizophrenia

Running title: Theta/Alpha Activity in Schizophrenia

Alexander Nakhnikian¹, Naoya Oribe^{1,2,3}, Shogo Hirano^{1,3}, Yuki Fujishima¹, Yoji Hirano^{1,3,4}, Paul G. Nestor⁵, Grace A. Francis¹, Margaret Levin⁶, Kevin M. Spencer¹

¹Neural Dynamics Laboratory, Research Service, VA Boston Healthcare System, and Department of Psychiatry, Harvard Medical School

²Department of Clinical Research, National Hospital Organization, Hizen Psychiatric Medical Center, Saga, Japan

³Department of Neuropsychiatry, Graduate School of Medical Sciences, Kyushu University

⁴Department of Psychiatry, Faculty of Medicine, University of Miyazaki, Miyazaki, Japan

⁵Department of Psychology, University of Massachusetts, Boston

⁶EPhysBio LLC

Acknowledgements

The work reported here was supported by grants I01 CX000154 (KMS) and I01 CX001443 (KMS) from the US Department of Veterans Affairs, and grants R01 MH080187 (KMS) and R01 MH093450 (ML, KMS) from the US National Institutes of Health.

Disclosures

KMS reported receiving consulting fees from Pacific Development and Technology LLC, Phenolaesis LLC, and Novartis Inc. in the past 3 years. ML is the Chief Executive Officer of EPhysBio LLC. None of the authors reported conflicts of interest.

Correspondence to:

Kevin M. Spencer, Ph.D.

VA Boston Healthcare System

150 S. Huntington Ave.

Boston, MA 02130

kevin.spencer.phd@proton.me

Abstract

Resting state electroencephalographic (EEG) activity in schizophrenia (SZ) is frequently characterized by increased power at slow frequencies, and/or a reduction of peak alpha frequency. Here we investigated the nature of these effects. As most studies to date have been limited by reliance on *a priori* frequency bands which impose an assumed structure on the data, we performed a data-driven analysis of resting EEG recorded in SZ patients and healthy controls (HC). The sample consisted of 39 chronic SZ and 36 matched HC. The EEG was recorded with a dense electrode array. Power spectral densities were decomposed via Varimax-rotated principal component analysis (PCA) over all participants and for each group separately. Spectral PCA was repeated at the cortical level on cortical current source density computed from standardized low resolution brain electromagnetic tomography. There was a trend for power in the theta/alpha range to be increased in SZ compared to HC, and peak alpha frequency was significantly reduced in SZ. PCA revealed that this frequency shift was due to the presence of a spectral component in the theta/alpha range (6-9 Hz) that was unique to SZ. The source distribution of this component involved mainly prefrontal and parahippocampal areas. Abnormal low frequency resting EEG activity in SZ was accounted for by a unique theta/alpha oscillation. Other reports have described a similar phenomenon suggesting that the neural circuits oscillating in this range are relevant to SZ pathophysiology.

Keywords: schizophrenia, resting state, electroencephalography, EEG, theta, alpha

Introduction

While stimulus- and task-evoked brain responses in individuals with schizophrenia (SZ) are frequently found to be reduced compared to healthy control participants (HC) (1), spontaneous brain activity, particularly measured with the electroencephalogram (EEG), is commonly found to be increased in SZ during the resting state. Increases in delta (~1-4 Hz) and/or theta (~5-8 Hz) power in SZ have been reported or are apparent in a number of studies (2-18; in ultra-high risk individuals, 19; in first-episode psychosis, 20) with observations going back many decades (21). Furthermore, a reduction in peak alpha frequency has also been reported, often in conjunction with increased theta/alpha power (10, 14, 22-25; in high vs. low schizotypy, 26). In contrast, changes in classical alpha band (8-13 Hz) power are inconsistent (2). The nature of paradoxically increased low frequency power in SZ is unclear and has received little investigation.

A limitation of most studies of resting state EEG in schizophrenia is that they rely on *a priori* -defined canonical frequency bands and thus impose an assumed structure on the data that might not accurately reflect the true spectral structure of effects. Data-driven approaches such as principal components analysis (PCA)

and independent component analysis (ICA) have the potential to overcome this problem by decomposing the EEG spectrum into characteristic spectral patterns in the data (11, 16-18), dissociating overlapping patterns of activity and revealing the true nature of effects.

Here we applied PCA in the spectral domain to investigate the nature of increased resting spectral power in schizophrenia. In particular, we were interested in determining whether decomposition of the power spectra would provide insights into the nature of increased low-frequency power and reduced peak alpha frequency in SZ. We hypothesized that increased power in the theta/alpha range in SZ could be due either to a reduction in the frequency of the same alpha generator in SZ as HC, or to the overlap of a distinct theta/alpha generator in SZ. To answer this question, we applied PCA with Varimax rotation to the power spectra of matched groups of SZ and HC in sensor space. We also applied Varimax-rotated PCA to the source-level spectra to determine the anatomical generators of theta/alpha activity in SZ.

Materials and Methods

Participants

The institutional review boards of the Veterans Affairs Boston Healthcare System and Harvard Medical School approved this study. SZ were recruited from the VA Boston Healthcare System Schizophrenia Center and HC were recruited from the Boston metropolitan area. All participants were right-handed. SZ were diagnosed with schizophrenia or schizoaffective disorder based on DSM-IV criteria following a standardized clinical interview. HC were excluded if they met SCID-Non-Patient edition criteria for an Axis-I disorder, or if they reported a first-degree relative with an Axis-I disorder. Exclusion criteria for all participants were: 1) past treatment with electroconvulsive therapy, 2) past major head trauma or a history neurological illness including epilepsy, 3) lifelong substance dependence or a history of substance abuse during the past 5 years, 4) estimated premorbid IQ (information subscale of the Wechsler Adult Intelligence Scale-IV [WAIS-IV]; 27) below 75. HC were matched to SZ at the group level on age, parental socioeconomic status (PSES; 28), gender proportion, and premorbid IQ. We assessed positive and negative symptoms using the Scale for the Assessment of Positive Symptoms (SAPS; 29) and the Scale for the Assessment of Negative Symptoms (SANS; 30). Chlorpromazine equivalent dosages were calculated using the methods of Stoll (31) and Woods (32).

We recorded EEG from 42 HC and 43 SZ. The data from 6 HC and 4 SZ were excluded to achieve age matching between groups. The final sample consisted of 36 HC and 39 SZ. See Table 1 for demographic and clinical data and group comparisons.

Prior to entering the study, participants were informed of the purpose of the experiment and the procedures employed. All participants provided written informed consent prior to enrollment. Participants were reimbursed for their participation in the study.

Procedures

Participants were seated comfortably in a quiet dim room. Resting-state EEG was recorded for 3 minutes during which participants were instructed to close their eyes and relax. The first 30 s of recording were discarded to ensure that the data reflected the participants being fully at rest.

EEG Recording and Processing

We recorded the EEG using an ActiveTwo system (Biosemi B.V.) with 71 sensors total, 68 channels to record brain signals and 3 for detecting eye movement. Signals were referenced to the systems' internal loop (CMS/DRL), sampled at 512 Hz, and bandpass filtered from 0.01 Hz to 103 Hz. DC offsets were kept below 25 mV during recordings. Bipolar vertical electro-oculograms were constructed from electrode Fp1 and an electrode below the left eye. The horizontal electro-oculogram was derived from sensors on the left and right outer canthi. Continuous EEG was epoched and filtered using BrainVision Analyzer 2.0.1 (Brain Products GmbH). Skin potentials and other slow artifacts were attenuated using a 0.1 Hz high-pass filter. Non-overlapping 1000 ms epochs were extracted for analysis. Power line noise at 60 Hz was reduced using

an in-house implementation of a spectral interpolation method (33) with the interpolation averaging range set to ± 2 Hz.

Further processing was performed in MATLAB (Mathworks, Inc) and IDL (L3Harris Geospatial Solutions, Inc.) using a combination of open-source third party software and in-house code. ICA, implemented using the EEGLAB (34) *runica.m* script, was used to remove ocular, cardiac, and muscle artifacts (35). ICs representing artifacts were visually identified based on topography, time series, and spectral signatures. Additional rejection criteria for a given epoch were: 1) $> \pm 90 \mu\text{V}$ at a single time point and 2) total amplitude range exceeding $|200| \mu\text{V}$. We retained data sets for which at least 75% of trials were free of range and eye movement artifacts following ICA. The average number of trials retained for HC was 134 and 137 for SZ. The number of retained trials did not differ between groups ($t_{73} = 0.90, p = 0.37$).

Spectral Analysis

Data were band-pass filtered from 0.1 to 100 Hz using a standard linear least squares algorithm, *eegfilt* from the EEGLAB toolbox. Sensor power spectral densities were computed using the Fast Fourier Transform with a Hann window. For each participant we pre-multiplied single-trial EEG from all channels by a periodic Hann window and then converted the data to frequency space via the Fast Fourier Transform. Tapered single-trial spectra were converted to power spectra by averaging twice the squared modulus of the Fourier coefficients across trials for all frequencies from 1 to 100 Hz. To obtain power spectral densities with physical units of $\mu\text{V}^2/\text{Hz}$ we divided each value by the sampling rate multiplied by the sum of squares of the taper.

PCA

To decompose the power spectra into their characteristic spectral patterns, we applied PCA to the data set, followed by Varimax rotation. The number of PCs retained for rotation was determined by inspection of the scree plot, retaining PCs up to and including the inflection in the plot, and equaled 5 for all PCAs reported here. These 5-PC solutions accounted for approximately 95% of total variance. Power spectral densities across both groups were concatenated into a single 5100 (75 participants X 68 sensors) by 100 (frequencies) data matrix (D). The Varimax solution was computed using code from the PCA Toolbox (36).

The first step was to obtain the 100 by 100 covariance matrix (C) among all frequencies along with its eigendecomposition. Let k be the number of factors. We then define the 100 by k loading matrix as $A = \Sigma^{-1}VP$. Σ contains the data standard deviation on the diagonals and is zero elsewhere and the rows of V are the first k eigenvectors of C . P is a diagonal matrix where each non-zero entry is the standard deviation of one of the rows of the score matrix DV . Principal component decomposition of source data (see below) proceeded as above except in this case D had 467925 (75 participants * 6239 voxels) rows. The vectors in the score and loading matrices were then recursively rotated seeking a solution as close as possible to the Varimax criterion of maximum variance among the squared loadings.

This approach maximally separates the factors while maintaining orthogonality. Maximal separation facilitates interpretation of the PCs, each corresponding to an observed variable or collection thereof; that is, each factor strongly correlates with variables it explains and weakly correlates with others. Orthogonality simplifies interpretation by eliminating possible correlations among factors but may be inappropriate if the factors are in fact strongly correlated. To account for this possibility, we repeated the analysis using Promax rotation, which allows for non-orthogonal results, and found that none of the components were significantly correlated when we relaxed the orthogonality restriction. Therefore, there was no benefit to utilizing the Promax solution.

Source Analysis

We performed source analysis to elucidate the distribution of brain-level generators giving rise to the effects observed in sensor space. Since it is not possible to localize PC scores directly, as these are not voltages, we localized the EEG data to source space and then performed a separate PCA on the source-level standardized current density estimation.

We consider the low-resolution brain electromagnetic tomography (LORETA) family of imaging solutions (37), which correct for spatial bias arising from the fact that EEG leadfields, as harmonic functions, which necessarily obtain their extreme values at the boundary points of their domain (38). Two variants of this method, standardized (sLORETA; 39) and exact (eLORETA; 40), can be shown to have zero localization error under the assumption that measurement and biological noise are independent. sLORETA, as the name implies, is a standardized estimator of source activity whereas eLORETA is a direct map from sensor space to brain-level current densities (i.e., a true inverse solution as opposed to a linear imaging technique). A drawback to eLORETA is that its zero bias condition only obtains under an assumption of structured noise that does not necessarily correspond to physical reality (40). Since sLORETA requires fewer constraints on the structure of measurement and biological noise in order to obtain spatially unbiased solutions, we chose it over the eLORETA modality.

Source analysis with the sLORETA procedure was carried out in the LORETA-KEY software system (v20201109). We computed the complex cross-spectral density matrices using built-in functions in LORETA-KEY. Data were tapered with a Hanning window and, for each participant, the spectral matrix for frequency ω is given by $S(\omega) = E[X(\omega)X(\omega)^*]$, where X is the Fourier transform of the signal in a column vector, $E[x]$ is the expected value of the enclosed variable, and “*” denotes complex conjugation and transposition. For each participant we used the multi-trial average of $X(\omega)X(\omega)^*$ as the sample estimator of $S(\omega)$. The standardized source image for frequency ω at the j th voxel is given by $T(j)S(\omega)T(j)^T$, where $T(j)$ is the (row) vector-valued imaging kernel.

The forward model was constructed in LORETA-KEY by registering standard electrode locations the MNI 152 structural magnetic resonance imaging (MRI) model with the leadfields restricted to cortical gray matter. To increase the stability of the solution, we applied adaptive Tikhonov regularization by setting the regularization parameter equal to 10% of the maximum eigenvalue of the leadfield Gram matrix; this approach ensures a degree of smoothing that increases the further the matrix deviates from an invertible matrix.

Statistics

For comparisons of power spectral densities as well as PC topographies and source distributions, we applied pair-wise independent samples t -tests using statistical non-parametric mapping (SnPM) with clustering correction for multiple comparisons (41). Power spectra and topographies were compared using in-house code. For source distributions we performed t -tests with SnPM maximum statistic controls for multiple comparisons as implemented in LORETA-KEY. For all in-house code, we validated our implementation by applying the code to random noise with the same structure as the experimental data 5000 times and confirming that the false positive rate was equal to the desired significance threshold, plus or minus a small amount of noise. All null distributions were based on 10,000 permutations of the empirical data.

At the sensor level we performed two-tailed t -tests while controlling for the number of sensors and number of PCs in tandem. Since the only significant difference we found was increased theta/alpha power in SZ (see Results), to determine the generating sources of this effect, we applied a one-tailed significance threshold to the source data and only included the theta/alpha component in the analysis. Our rationale for a less conservative test was three-fold. First, we were interested only in localizing the theta/alpha sources, not in hypothesis testing. Second, there was no reason to expect the direction of the effect to be reversed from the sensor to source level. Third, LORETA-KEY applies a voxel-wise control, which is necessary in order to identify single-voxel effects above chance, but is also more conservative than the cluster-wise control we applied in sensor space (41). We therefore chose a one-tailed test on a single PC in order to reduce the risk of Type II error under the assumption that increasing the probability of Type I error is minimal given these three considerations.

To assess possible group differences in peak alpha frequency and power we identified the maximum power value in the 5-20 Hz range and the corresponding peak frequency for all participants. Group differences for both measures were tested using independent-samples t -tests.

Sex was compared between groups using the χ^2 test. Spearman’s ρ was used for all correlations. Statistical

corrections for multiple tests were applied as noted in the Results. For all statistical analyses, $\alpha = 0.05$ and tests were 2-tailed except as noted.

Results

Raw Power Spectra Differences

First we averaged the power spectra over all the electrodes and performed cluster permutation analysis to determine if there were overall group differences across frequencies. SZ exhibited a trend towards increased power compared to HC (cluster $p = 0.06$, 2-tailed) in the upper theta/lower alpha range (7-9 Hz) (Fig. 1). Peak alpha frequency was significantly decreased in SZ (8.9 Hz) compared to HC (9.7 Hz) ($t_{73}=2.8453$, $p = 0.005$, 2-tailed) with no difference in peak alpha power ($t_{73} = -1.5574$, $p = 0.12$).

Sensor-Level PCAs

Global decomposition. The first PCA was done across both HC and SZ data sets at the sensor level. To visualize the contributions of the PCs to the data, we plotted the PC loadings (correlations between PCs and original variables) weighted by the standard deviations of the original variables, which preserves the structure of the PC weights in the original data space. The percentages of variance accounted for by the PCs are given in Table 2.

The results of the global PCA are presented in Fig. 2. PC1 was maximal at 1 Hz and decayed rapidly with power vanishing at the upper delta bound (~ 4 Hz), with largest scores at temporal sensors. PC2 peaked at 10 Hz and covered the canonical alpha band (8-13 Hz) with maximum scores at bilateral occipital sites. PC3 peaked at 7-8 Hz with a band covering theta/alpha frequencies (6-9 Hz) and scores maximized at lateral occipital and occipito-temporal sensors. PC4 peaked at 9 Hz and was similar to PC2 in scalp distribution. PC5 exhibited a biphasic loading pattern with a peak covering high theta through low alpha (6-9 Hz) and a trough at 10 Hz. This PC also exhibited the lowest loading values, suggesting a noise PC. We retained it since it corresponded to the bend in the scree plot. The spatial distribution of this PC's scores was focused on bilateral occipital sites.

For each scalp PC, the scores were compared between HC and SZ using SnPM as described above. We found a significant difference between HC and SZ scores only for PC 3 (6-9 Hz), which accounted for the theta/alpha effect in the raw data. There was one significant sensor cluster ($p = 0.002$) that covered the entire scalp except for the central parietal and temporal regions.

Within-group decompositions. Next, to determine if the theta/alpha activity represented by PC3 was present in both participant groups or unique to SZ, we applied PCA to the HC and SZ data sets separately. The overall spectral and topographic patterns in the within-group decompositions were generally similar (Fig. 3) except as noted below. In HC (Fig. 3A/B), PC1 exhibited a prominent delta peak (1-3 Hz) with scores maximized at temporal sites. PC2 and PC3 both peaked at alpha (~ 10 Hz) and had maximum score values at bilateral occipital sites, with PC2 focused over more medial sites than PC3. PC4 did not exhibit a distinct spectral structure while PC5 exhibited a bimodal alpha peak focused at midline occipital sites.

In SZ, PC1 was almost identical to HC PC3 in spectral and topographic structure. PC2 exhibited a distinct theta/alpha (6-9 Hz) and lateral occipito-temporal topography similar to PC3 in the global decomposition. SZ PC3 accounted for lateral temporal delta activity, as in HC PC1. SZ PC4 and PC5 had mixed spectral structures with weak and relatively unstructured scalp distributions.

Thus, it appears that the theta/alpha activity observed in SZ in the raw data, and which was accounted for by PC3 in the global decomposition, may constitute a unique pattern of activity in SZ, as there was no counterpart of SZ PC2 in the HC decomposition.

Source-Level PCA

To determine the cortical sources of the theta/alpha activity identified in sensor space for SZ, we transformed the scalp voltage data to cortical current source density using sLORETA (see Methods) and applied PCA

to the resulting data. The spectral patterns at the source level were similar to those we found in sensor space global PCA, with distinct components corresponding to delta, alpha, and theta/alpha bands (Fig. 4). Theta/alpha activity was represented by PC2 (6-7 Hz peak), which had a broad spatial distribution across occipital, parietal, temporal, and lateral frontal cortex, with greater values in the right hemisphere. The HC vs. SZ contrast for PC2 (Fig. 4D) showed significantly increased activity ($p < 0.05$) in SZ compared to HC predominantly in the left middle frontal gyrus (Brodmann areas 6, 8, and 9) but also over a collection of voxels including the inferior frontal gyrus, parahippocampal gyrus, and precentral gyrus. The complete set of significant voxels is given in Table 3.

The rest of the source-level PCs were also very similar to the sensor-level PCs. PC1 (alpha) peaked at 9 Hz with a source distribution that included ventral prefrontal, temporal, and lateral occipital cortex, predominantly in the right hemisphere. PC3 accounted for delta (1-3 Hz) power and was most prominent in widespread posterior areas of the left hemisphere with some bilateral occipital activation. PC4 was a second alpha component that peaked at 10 Hz with its most prominent activations in the right lateral frontal and parieto-occipital cortices. PC5 had a multi-phasic spectral structure with peaks in the theta and alpha bands, smaller loadings, and smaller scores, which were most prominent in the left fronto-temporal cortex. The percentage of variance accounted for by all the PCs is summarized in Table 2.

Symptom Correlations

Average scores for the sensor-level SZ theta/alpha component (SZ PC3) did not differ significantly correlate with any of the symptom rating scales at uncorrected p levels. We did not assess source estimate correlations with symptom scores as we found no significant correlations at the sensor level.

Discussion

Overview

In the raw power spectra, the alpha peak was downwardly shifted in frequency in SZ relative to HC, manifesting as a trend-level increase in spectral power in the 7-9 Hz range and a significant reduction in peak frequency from ~ 10 to ~ 9 Hz in SZ compared to HC. PCA decomposed the data into a small number of characteristic spectral patterns, among which only the theta/alpha PC showed a significant difference between groups, with greater power in SZ relative to HC. When the SZ and HC data were analyzed separately with spectral PCA, the theta/alpha PC was apparent only in the SZ data. Localization of the theta/alpha activity with sLORETA revealed that this activity in SZ was widely distributed across the cortex, mainly in the prefrontal cortex, with a maximum in the left middle frontal gyrus. Thus, our results suggest that in SZ, a distinct set of theta/alpha generators is active that is not apparent in healthy individuals.

Spectral Features of Resting EEG in SZ

Increased power in the schizophrenia spectrum during the resting state in the theta or theta/alpha ranges has been reported in a number of studies (e.g., 2-21). However, in contrast to some studies, we did not also find significantly increased delta power (4, 9-12, 15-18), which highlights the heterogeneity of spectral profiles observed in SZ (2). One possible explanation is that the separation of power spectra evident in the delta and low theta bands in Fig. 1 would be significant with a larger sample size. Alternatively, it is possible that such an effect was simply not present in this particular patient sample. Furthermore, we did not find a group difference in alpha power, although this is not surprising as evidence of reduced resting alpha in SZ is far less consistent than evidence of augmented delta and theta power (2).

The reduction of peak alpha frequency or “slowing” of the EEG reported in some studies (e.g., 10, 14, 22-25) may actually be due to increased theta/alpha power (global sensor PC3) overlapping with “classical” alpha oscillations (here represented by PC2 and PC4 in the global sensor PCA). If the classical alpha oscillations do not differ in power between SZ and HC, the addition of the theta/alpha oscillation could cause the apparent single alpha peak to shift downwards in frequency. The further use of spectral decomposition methods like PCA or ICA will be necessary to determine whether this is the case.

Our analyses suggest that the theta/alpha oscillation is unique to SZ because a PC representing this oscillation was not present in the decomposition of the HC data, only in the SZ data. The uniqueness of the theta/alpha oscillation to SZ may be supported by the finding of Narayanan et al. (11) that the power of a theta/alpha IC in their study was not only significantly increased in SZ compared to HC, but also significantly correlated with the Schizophrenia-Bipolar Scale, such that the IC had higher values for SZ than psychotic bipolar patients.

Sensor vs. Source-Level Results

In keeping with results obtained at the sensor level we found that in source space the only significant differences between HC and SZ were accounted for by the theta/alpha component. In contrast to our sensor results, at the source level the spatial extent of the group difference was confined to the left frontal cortex. This discrepancy between source and sensor power raises a number of interesting issues that warrant further investigation. The first consideration is methodological. The advantage of LORETA-KEY's implementation of the maximum statistic approach for SnPM correction is that it allows us to localize effects to individual voxels. This comes at the cost of somewhat reduced statistical power compared to the cluster correction approach we employed at the sensor level (41), which could account for some changes in the spatial profile of the effect at the sensor versus source level. That said, we explored this possibility by repeating the sensor analysis using max-stat as opposed to cluster correction (data not shown) and though the spatial extent of the effect was slightly reduced, the overall effect at both frontal and occipital sites was still clearly present. It is worth noting that the overall distribution of t -scores at the source level was similar to that observed at the sensor level, with peaks at frontal and occipital sites, though only the left frontal effects passed multiple comparisons correction.

It is also worth noting that, although the source scores were above chance across the brain with a distribution consistent with the observed sensor scores, the maximum t scores were much more focal at the source level and concentrated over the left frontal cortex. This could be an issue of statistical power. Some amount of spatial jitter is inevitable when performing electromagnetic brain imaging, especially when using template forward models, and increased spatial noise could reduce power in source space. Furthermore, LORETA-KEY only implements the maximum voxel variant of SnPM, and as noted above, this approach achieves greater spatial specificity at the cost of reduced power. This does not of course directly imply that cluster correction at the source-level would return the same result and further research using single-subject MRI and sensor grids would clarify the issue of spatial jitter by increasing the accuracy of the source model. Conversely, it is possible that frontal sites are a driver of aberrant theta/alpha activity throughout the brain in SZ and that this more focal effect is only apparent in source space. Network theoretic analysis using functional and effective connectivity measures are necessary to investigate this possibility.

Mechanistic Considerations

Increased theta/alpha activity in SZ was mainly found across a wide swath of the prefrontal cortex and the parahippocampal cortex, with a statistical maximum spanning Brodmann areas 6, 8, and 9 in the middle frontal gyrus. Dysfunction of the prefrontal cortex in schizophrenia has been long-established (e.g., 39, 40). At the microcircuit level, reduced glutamatergic inputs to pyramidal cells (44) and reduced function of parvalbumin-expressing (PV), fast-spiking inhibitory interneurons (45) are prominent features in schizophrenia. While it is thought to be understood how these abnormalities affect gamma band (30-100 Hz) oscillations in SZ (e.g., 46), it is not clear how theta/alpha activity might be affected. Indeed, we do not know if the 6-9 Hz oscillation should be considered as a theta or an alpha oscillation, or possibly as a separate, distinct oscillation.

If this theta/alpha oscillation is part of the family of alpha oscillations, the microcircuit interactions underlying these oscillations are poorly understood. Alpha oscillations are generated both in the neocortex and in the thalamus and involve cortico-thalamic interactions (e.g., 47). An increase in theta/alpha oscillation power has been reported in several neuropsychiatric disorders (14) as part of the more general syndrome of thalamocortical dysrhythmia (48).

On the other hand, if the 6-9 Hz theta/alpha oscillation could be considered as part of the family of theta oscillations, there is more hope, as the circuit mechanisms underlying theta oscillations have been well-studied in the hippocampus. Theta oscillations in the hippocampus involve reciprocal interactions between pyramidal cells, PV interneurons, and slower spiking interneurons. Dysfunction in PV interneurons leads to reductions in theta power and synchronization (49), as well as reduced phase-amplitude coupling between theta and gamma oscillations (50). But since theta/alpha power was increased here, it seems unlikely that the PV interneuron dysfunction that characterizes SZ, in which it is associated with decreased evoked gamma oscillations and increased spontaneous gamma activity (e.g., 51), could also produce increased theta/alpha activity.

We note that previously our group reported increased cross-frequency coupling in SZ between upper theta (7.24 to 8.74 Hz) phase and alpha (9.99 to 11.2 Hz) amplitude in the EEG recorded during the resting state and auditory steady state stimulation, which was localized to auditory cortex (52). Since the central frequency of the phase component identified in that study was within the bandwidth of the theta/alpha component reported here, it is possible that that effect and the present theta/alpha oscillation are related. We will investigate this question in future work.

As reduced function of *N*-methyl-D-aspartate receptors (NMDARs) has been implicated in the pathogenesis of schizophrenia (53), research on the effects of NMDAR antagonists on the EEG could provide insights into the nature of theta/alpha activity in SZ. Interestingly, studies of the effects of ketamine on the resting EEG of healthy individuals generally have reported reductions in alpha power (54-56), but in some cases elevated mid-frontal theta power (55, 57). However, effects similar to the theta/alpha component found here have not been reported in ketamine studies, to our knowledge. This discrepancy suggests that the acute ketamine model does not fit all of the electrophysiological abnormalities that are characteristic of SZ, at least in the chronic state (e.g., 58).

Finally, we note that increased spontaneous low-frequency (delta and theta) activity in SZ has been related to dopamine metabolism mediated by the catechol-*O*-methyl transferase (COMT) gene (18, 59). It is not clear whether those effects extended in the power spectrum into the theta/alpha range, however.

Limitations

Several limitations of this study should be considered when interpreting the results. All patients in this study were in the chronic state and were receiving antipsychotic medication, so it is unclear to what extent our findings might have been influenced by antipsychotics or chronicity, although we found no correlations between theta/alpha power and antipsychotic dosage. Although this study benefited from the use of a dense electrode grid, we did not record individual sensor locations or structural MRI, thus the spatial accuracy of our source model is lower than what we would obtain with individual forward models. Finally, the application of other spectral decomposition methods besides PCA/Varimax, as used here, may provide additional insight into the composition of resting-state spectra in schizophrenia.

Conclusion

A large number of papers have reported that in the resting state, individuals with schizophrenia-spectrum disorders show an increase in low frequency EEG activity. Here we used a spectral decomposition method to find that this activity was accounted for by an apparently unique theta/alpha oscillation in SZ, which was present in widespread areas of the neocortex. The circuit basis for this increased theta/alpha activity in SZ is unknown. Further research into the mechanisms underlying alpha and theta oscillations is warranted to elucidate the mechanisms underlying this effect.

References

1. Javitt DC, Spencer KM, Thaker GK, Winterer G, Hajós M (2008): Neurophysiological biomarkers for drug development in schizophrenia. *Nat Rev Drug Discov* 7: 68–83.
2. Boutros NN, Arfken C, Galderisi S, Warrick J, Pratt G, Iacono W (2008): The status of spectral EEG abnormality as a diagnostic test for schizophrenia. *Schizophr Res* 99: 225–237.

3. Cecchi M *et al.* (2023). Validation of a suite of ERP and QEEG biomarkers in a pre-competitive, industry-led study in subjects with schizophrenia and healthy volunteers. *Schizophr Res*254:178–189.
4. Clementz, B., Sponheim, S., Iacono, W. G., Beiser M (1994): Resting EEG in first-episode schizophrenia patients, bipolar psychosis patients, and their first-degree relatives. *Psychophysiology*31: 486–494.
5. Garakh Z, Zaytseva Y, Kapranova A, Fiala O, Horacek J, Shmukler A, *et al.* (2015): EEG correlates of a mental arithmetic task in patients with first episode schizophrenia and schizoaffective disorder. *Clin Neurophysiol* 126: 2090–2098.
6. Hanslmayr S, Backes H, Straub S, Popov T, Langguth B, Hajak G, *et al.* (2013): Enhanced resting-state oscillations in schizophrenia are associated with decreased synchronization during inattentive blindness. *Hum Brain Mapp* 34: 2266–2275.
7. Hong LE, Summerfelt A, Mitchell BD, O’Donnell P, Thaker GK (2012). A shared low-frequency oscillatory rhythm abnormality in resting and sensory gating in schizophrenia. *Clin Neurophysiol*123:285–292.
8. Kim JS, Shin KS, Jung WH, Kim SN, Kwon JS, Chung CK (2014): Power spectral aspects of the default mode network in schizophrenia: an MEG study. *BMC Neurosci* 15: 104.
9. Kim M, Lee TH, Park H, Moon SY, Lho SK, Kwon JS (2022). Thalamocortical dysrhythmia in patients with schizophrenia spectrum disorder and individuals at clinical high risk for psychosis. *Neuropsychopharmacol* 47: 673–680.
10. Koshiyama D, Miyakoshi M, Tanaka-Koshiyama K, Joshi YB, Sprock J, Braff DL, Light GA (2021): Abnormal phase discontinuity of alpha- and theta-frequency oscillations in schizophrenia. *Schizophr Res*231: 73–81.
11. Narayanan B, O’Neil K, Berwise C, Stevens MC, Calhoun VD, Clementz BA, *et al.* (2014). Resting state electroencephalogram oscillatory abnormalities in schizophrenia and psychotic bipolar patients and their relatives from the bipolar and schizophrenia network on intermediate phenotypes study. *Biol Psychiatry* 76: 456–465.
12. Ranlund S, Nottage J, Shaikh M, Dutt A, Constante M, Walshe M, *et al.* (2014): Resting EEG in psychosis and at-risk populations - a possible endophenotype? *Schizophr Res* 153: 96–102.
13. Razavi N, Jann K, Koenig T, Kottlow M, Hauf M, Strik W, Dierks T (2013): Shifted coupling of EEG driving frequencies and fMRI resting state networks in schizophrenia spectrum disorders. *PLoS ONE* 8: e76604.
14. Schulman JJ, Cancro R, Lowe S, Lu F, Walton KD, Llinás RR (2011). Imaging of thalamocortical dysrhythmia in neuropsychiatry. *Front Hum Neurosci* 5: 69.
15. Siekmeier PJ, Stufflebeam SM (2010): Patterns of spontaneous magnetoencephalographic activity in patients with schizophrenia. *J Clin Neurophysiol* 27: 179–190.
16. Sponheim SR, Clementz BA, Iacono WG, Beiser M (1994): Resting EEG in first-episode and chronic schizophrenia. *Psychophysiology* 31: 37–43.
17. Sponheim SR, Clementz BA, Iacono WG, Beiser M (2000): Clinical and biological concomitants of resting state EEG power abnormalities in schizophrenia. *Biol Psychiatry* 48: 1088–1097.
18. Venables NC, Bernat EM, Sponheim SR (2009): Genetic and disorder-specific aspects of resting state EEG abnormalities in schizophrenia. *Schizophr Bull* 35: 826–839.
19. Sollychin M, Jack BN, Polari A, Ando A, Amminger GP, Markulev C, *et al.* (2019): Frontal slow wave resting EEG power is higher in individuals at Ultra High Risk for psychosis than in healthy controls but is not associated with negative symptoms or functioning. *Schizophr Res* 208: 293–299.
20. Gawne TJ, Overbeek GJ, Killen JF, Reid MA, Kraguljac NV, Denney TS, Ellis CA, Lahti AC (2020). A multimodal magnetoencephalography 7 T fMRI and 7 T proton MR spectroscopy study in first episode psychosis. *npj Schizophr* 6:23.
21. Itil TM (1977): Qualitative and quantitative EEG findings in schizophrenia. *Schizophr Bull* 3: 61–79.
22. Cañive JM, Lewine JD, Edgar JC, Davis JT, Torres F, Roberts B, *et al.* (1996): Magnetoencephalographic assessment of spontaneous brain activity in schizophrenia. *Psychopharmacol Bull* 32: 741–750.
23. Goldstein MR, Peterson MJ, Sanguinetti JL, Tononi G, Ferrarelli F (2015): Topographic deficits in alpha-range resting EEG activity and steady state visual evoked responses in schizophrenia. *Schizophr Res* 168: 145–152.

24. Murphy M, Öngür D (2019): Decreased peak alpha frequency and impaired visual evoked potentials in first episode psychosis. *NeuroImage Clin* 22: 101693.
25. Ramsay IS, Lynn P, Schermitzler B, Sponheim S (2021): Individual alpha peak frequency is slower in schizophrenia and related to deficits in visual perception and cognition. *Sci Rep* 11: 17852.
26. Fuggetta G, Bennett MA, Duke PA, Young AMJ (2014). Quantitative electroencephalography as a biomarker for proneness toward developing psychosis. *Schizophrenia Res* 153: 68–77.
27. Wechsler D (2008): *Wechsler Adult Intelligence Scale-Fourth Edition* . San Antonio, TX: Pearson.
28. Hollingshead A (1965): *A Two Factor Index of Social Position* . New Haven, Connecticut: Yale University Press.
29. Andreasen NC (1984): Scale for the Assessment of Positive Symptoms (SAPS). Iowa City, IA: University of Iowa.
30. Andreasen NC (1983): Scale for the Assessment of Negative Symptoms (SANS). Iowa City, IA: University of Iowa.
31. Stoll A (2001): The Psychopharmacology Reference Card. Belmont, MA: Mclean Hospital.
32. Woods SA (2003): Chlorpromazine equivalent doses for the newer atypical antipsychotics. *J Clin Psychiatry* 64: 663–667.
33. Leske S, Dalal SS (2019): Reducing power line noise in EEG and MEG data via spectrum interpolation. *NeuroImage* 189: 763–776.
34. Delorme A, Makeig S (2004): EEGLAB: An open source toolbox for analysis of single-trial EEG dynamics including independent component analysis. *J Neurosci Methods* 134: 9–21.
35. Delorme A, Sejnowski T, Makeig S (2007): Enhanced detection of artifacts in EEG data using higher-order statistics and independent component analysis. *Neuroimage* 34: 1443–1449.
36. Dien J (2010): The ERP PCA Toolkit: An open source program for advanced statistical analysis of event-related potential data. *J Neurosci Methods* 187: 138–145.
37. Pascual-Marqui RD, Michel CM, Lehmann D (1994): Low resolution electromagnetic tomography: a new method for localizing electrical activity in the brain. *Int J Psychophysiol* 18: 49–65.
38. Pascual-Marqui RD (1999): Review of methods for solving the EEG inverse problem. *Int J Bioelectromagn* 1: 75–86.
39. Pascual-Marqui RD (2002): Standardized low resolution brain electromagnetic tomography (sLORETA): technical details. *Methods Find Exp Clin Pharmacol* 24D: 5–12.
40. Pascual-Marqui RD (2007): Discrete, 3D distributed, linear imaging methods of electric neuronal activity. Part 1: exact, zero error localization [Mathematical Physics; Mathematical Physics; Biological Physics; Neurons and Cognition]. *arXiv: 07103341* 1–16.
41. Maris E, Oostenveld R (2007): Nonparametric statistical testing of EEG- and MEG-data. *J Neurosci Methods* 164: 177–190.
42. Lesh TA, Niendam TA, Minzenberg MJ, Carter CS (2011): Cognitive control deficits in schizophrenia: Mechanisms and meaning. *Neuropsychopharmacology* 36: 316–338.
43. Weinberger DR (1988): Schizophrenia and the frontal lobe. *Trends Neurosci* 11: 367–370.
44. Konopaske GT, Lange N, Coyle JT, Benes FM (2014): Prefrontal cortical dendritic spine pathology in schizophrenia and bipolar disorder. *JAMA Psychiatry* 71:1323–1331.
45. Lewis DA, Curley AA, Glausier JR, Volk DW (2012): Cortical parvalbumin interneurons and cognitive dysfunction in schizophrenia. *Trends Neurosci* 35: 57–67.
46. Gonzalez-Burgos G, Lewis DA (2012): NMDA receptor hypofunction, parvalbumin-positive neurons, and cortical gamma oscillations in schizophrenia. *Schizophr Bull* 38:950–957.
47. Halgren M, Ulbert I, Bastuji H, Fabó D, Eróss L, Rey M, Devinsky O, Doyle WK, Mak-McCully R, Halgren E, Wittner L, Chauvel P, Heit G, Eskandar E, Mandell A, Cash SS (2019): The generation and propagation of the human alpha rhythm. *Proc Natl Acad Sci USA* 116:23772–23782.
48. Llinás R, Urbano FJ, Leznik E, Ramírez RR, van Marle HJF (2005): Rhythmic and dysrhythmic thalamocortical dynamics: GABA systems and the edge effect. *Trends Neurosci* 28:325–333.
49. Cobb SR, Buhl EH, Halasy K, Paulsen O, Somogyi P (1995): Synchronization of neuronal activity in hippocampus by individual GABAergic interneurons. *Nature* 378: 75–78.

50. Tort ABL, Rotstein HG, Dugladze T, Gloveli T, Kopell NJ (2007): On the formation of gamma-coherent cell assemblies by oriens lacunosum-moleculare interneurons in the hippocampus. *Proc Natl Acad Sci USA* 104: 13490–13495.
51. Hirano Y, Oribe N, Kanba S, Onitsuka T, Nestor PG, Spencer KM (2015): Spontaneous gamma activity in schizophrenia. *JAMA Psychiatry* 72:813–821.
52. Hirano S, Nakhnikian A, Hirano Y, Oribe N, Kanba S, Onitsuka T, Levin M, Spencer KM (2018): Phase-amplitude coupling of the electroencephalogram in the auditory cortex in schizophrenia. *Biol Psychiatry Cogn Neurosci Neuroimaging* 3: 69–76.
53. Javitt DC, Zukin S. (1991): Recent advances in the phencyclidine model of schizophrenia. *Am J Psychiatry* 148: 1301–1308.
54. de la Salle S, Choueiry J, Shah D, Bowers H, McIntosh J, Ilivitsky V, Knott V (2016): Effects of ketamine on resting-state EEG activity and their relationship to perceptual/dissociative symptoms in healthy humans. *Front Pharmacol* 7: 348.
55. Muthukumaraswamy SD, Shaw AD, Jackson LE, Hall J, Moran R, Saxena N (2015): Evidence that sub-anesthetic doses of ketamine cause sustained disruptions of NMDA and AMPA-mediated frontoparietal connectivity in humans. *J Neurosci* 35: 11694–11706.
56. Pallavicini C, Vilas MG, Villarreal M, Zamberlan F, Muthukumaraswamy S, Nutt D, *et al.* (2019): Spectral signatures of serotonergic psychedelics and glutamatergic dissociatives. *NeuroImage* 200: 281–291.
57. Curic S, Andreou C, Nolte G, Steinmann S, Thiebes S, Polomac N, *et al.* (2021). Ketamine alters functional gamma and theta resting-state connectivity in healthy humans: Implications for schizophrenia treatment targeting the glutamate system. *Front Psychiatry* 12: 671007.
58. Anticevic A, Corlett PR, Cole MW, Savic A, Gancsos M, Tang Y, Repovs G, Murray JD, Driesen NR, Morgan PT, Xu K, Wang F, Krystal JH (2015). N-methyl-D-aspartate receptor antagonist effects on prefrontal cortical connectivity better model early than chronic schizophrenia. *Biol Psychiatry* 77:569–580.
59. Winterer G, Egan MF, Kolachana BS, Goldberg TE, Coppola R, Weinberger DR (2006). Prefrontal electrophysiologic “noise” and catechol-O-methyltransferase genotype in schizophrenia. *Biol Psychiatry* 60: 578–584.

Table 1. Demographic data and group comparisons. Means (standard error) are reported. For race, W = white, B = Black, and A = Asian (following US government definitions). No participants were Latino.

	HC	SZ	Group Comparison
N	36	39	-
Age	44.9 (1.2)	45.0 (1.5)	$t_{73} = -0.045, p = 0.96$
Sex (F/M)	10/26	8/31	$U_{75} = 753, p = 0.47$
Race (A/B/W)	1/11/24	2/14/23	$U_{74} = 633, p = 0.524$
PSES (HC/SZ)	2.4 (0.2)	2.76 (0.2)	$t_{70} = -1.30, p = 0.20$
WAIS-IV Info	104.1 (2.3)	99.3 (2.0)	$t_{73} = 1.59, p = 0.12$
SAPS	-	9.51 (0.61)	-
SANS	-	9.73 (0.92)	-
Chlorpromazine equivalents	-	393.22 (64.94)	-

Table 2. Percentage of variance accounted for by each component in the PCAs on sensors and sources, global and for each group separately.

PC	Sensor/Global	Sensor/HC	Sensor/SZ	Source/Global
1	56.5%	59.3%	55.8%	47.0%
2	20.0%	19.7%	22.0%	17.7%

PC	Sensor/Global	Sensor/HC	Sensor/SZ	Source/Global
3	14.0%	14.1%	16.0%	13.5%
4	5.1%	2.3%	3.0%	8.7%
5	1.9%	1.4%	1.3%	4.4%

Table 3. Anatomical locations and number/percentage of voxels above chance at the 0.05 and 0.01 levels of significance for the SZ > HC theta/alpha effect.

Anatomical Label	Brodmann Areas ($p < 0.05$)	# Voxels ($p < 0.05$)	Brodmann Areas ($p < 0.01$)
Middle Frontal Gyrus	6, 8, 9, 10,11, 46, 47	108 (27%)	6, 8, 9
Parahippocampal Gyrus	27, 28, 30, 34, 35, 36, 37	84 (21%)	
Inferior Frontal Gyrus	6, 9, 10, 44, 45, 46, 47	74 (19%)	
Precentral Gyrus	4, 6, 9, 44	48 (12%)	6
Uncus	20, 28, 34, 36, 38	33 (8%)	
Fusiform Gyrus	20, 26, 37	19 (5%)	
Inferior Temporal Gyrus	20	9 (2%)	
Superior Frontal Gyrus	8,10	6 (2%)	
Subcallosal Gyrus	25,34	5 (1%)	
Medial Frontal Gyrus	25	3 (<1%)	
Anterior Cingulate	25	2 (<1%)	
Sub-Gyral	10	1 (<1%)	
Superior Temporal Gyrus	38	1 (<1%)	

Figure Legends

Fig. 1: Power spectral densities \pm SEM for both healthy controls (HC) and schizophrenia patients (SZ) averaged across sensors. Cluster corrected t -tests revealed a significant difference in the theta/alpha range (7-9 Hz), which is indicated by the green box. Peak alpha frequency was significantly decreased in SZ compared to HC.

Fig. 2: Sensor-level global PCA results. **(A)** Spectral loadings weighted by variable standard deviations (see Methods). PC3 accounts for the theta/alpha difference apparent in the sensor-level grand average (Fig. 1A). The other PCs account for delta (PC1) and alpha activities (PCs 2, 4, and 5). **(B, C)** Global PC score topographies for **(B)** HC and **(C)** SZ. **(D)** Topographies of t -scores of the HC minus SZ effect. Red sensor markers indicate significant differences with cluster-correction at $p < 0.05$ (2-tailed). The only PC for which we observed significant differences between groups was PC3 (theta/alpha). There were two significant sensor clusters, one over frontal sites and a second over medial occipital and posterior parietal sites.

Fig. 3: Results for the individual sensor-level HC and SZ PCAs. **(A)** HC PCA spectral loadings (weighted as in Fig. 2). **(B)** HC PCA score topographies. **(C)** SZ PCA spectral loadings (weighted). **(D)** SZ PCA score topographies. SZ PC2 corresponds to the theta/alpha PC (PC3) found in the global sensor-level PCA (Fig. 2).

Fig. 4: Source-level PCA results. **(A)** Weighted spectral loadings. PC2 corresponds to the theta/alpha PC3 in the sensor-level global PCA. **(B, C)** PC score distributions for **(B)** HC and **(C)** SZ. Dorsal views of the inflated cortical surface are shown. The color bar indicates PC score values. **(D)** Anatomical distribution of HC minus SZ t scores for PC2. Voxels for which the contrast was significant (following max-stat correction) are colored (range is $-3.3 < t < -2.7$). Dorsal (left) and ventral (right) views of the inflated cortical surface are shown.

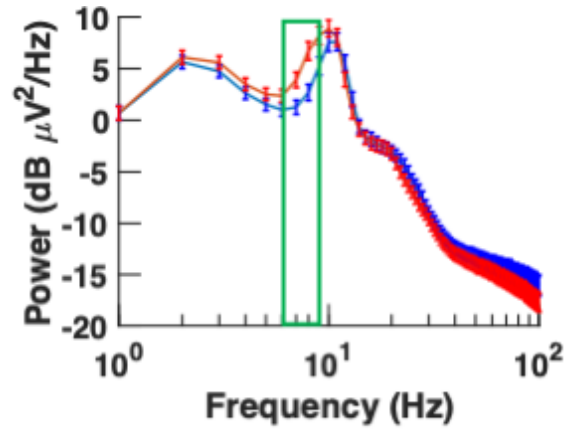


Fig. 1: Power spectral densities \pm SEM for both healthy controls (HC) and schizophrenia patients (SZ) averaged across sensors. Cluster corrected *t*-tests revealed a significant difference in the theta/alpha range (7-9 Hz), which is indicated by the green box. Peak alpha frequency was significantly decreased in SZ compared to HC.

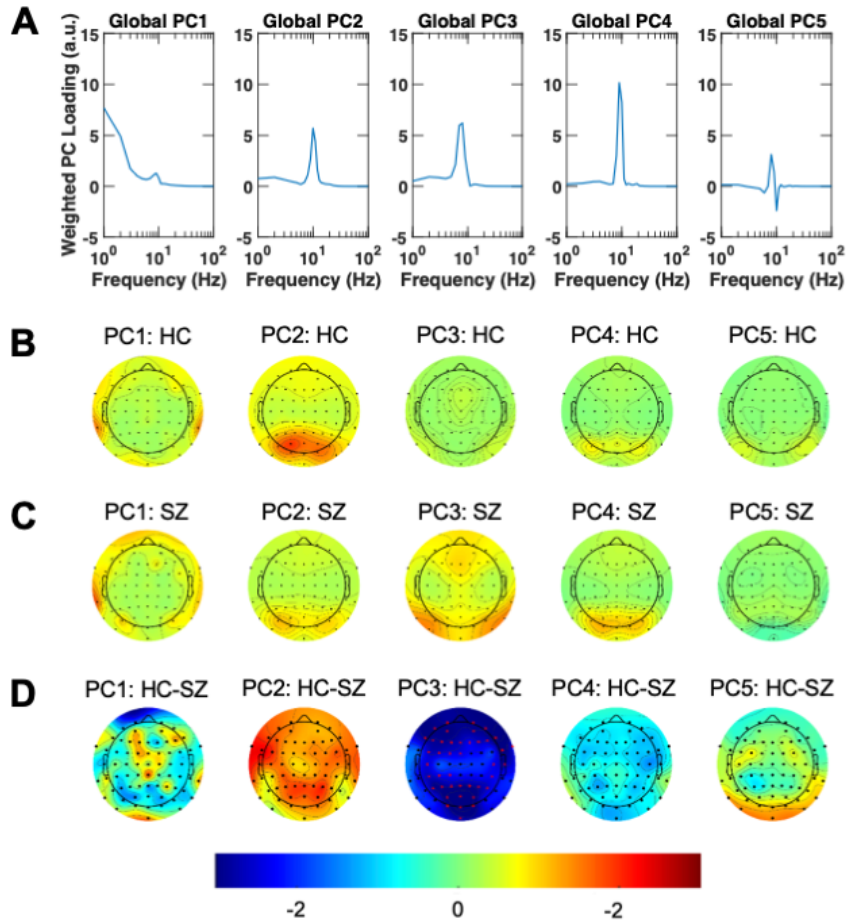


Fig. 2. Sensor-level global PCA results. (A) Spectral loadings weighted by variable standard deviations (see Methods). PC3 accounts for the theta/alpha difference apparent in the sensor-level grand average (Fig. 1A). The other PCs account for delta (PC1) and alpha activities (PCs 2, 4, and 5). (B, C) Global PC score topographies for (B) HC and (C) SZ. (D) Topographies of t-scores of the HC minus SZ effect. Red sensor markers indicate significant differences with cluster-correction at $p < 0.05$ (2-tailed). The only PC for which we observed significant differences between groups was PC3 (theta/alpha). There were two significant sensor clusters, one over frontal sites and a second over medial occipital and posterior parietal sites.

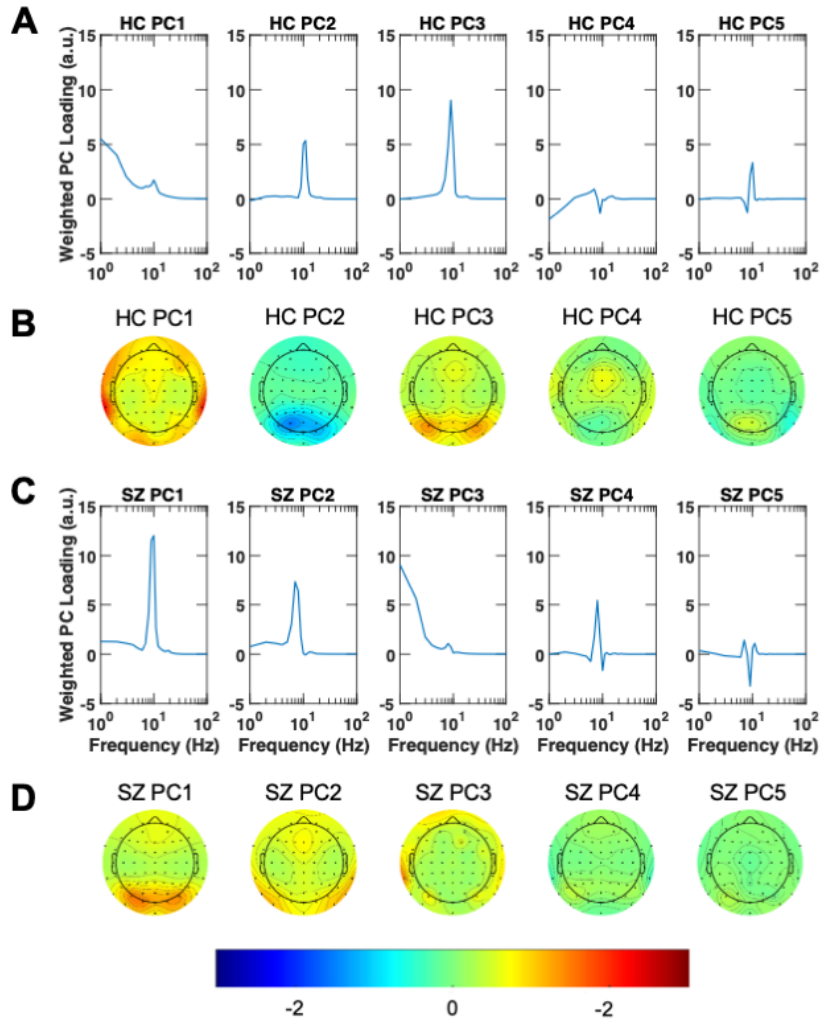


Fig. 3: Results for the individual sensor-level HC and SZ PCAs. **(A)** HC PCA spectral loadings (weighted as in Fig. 2). **(B)** HC PCA score topographies. **(C)** SZ PCA spectral loadings (weighted). **(D)** SZ PCA score topographies. SZ PC2 corresponds to the theta/alpha PC (PC3) found in the global sensor-level PCA (Fig. 2).

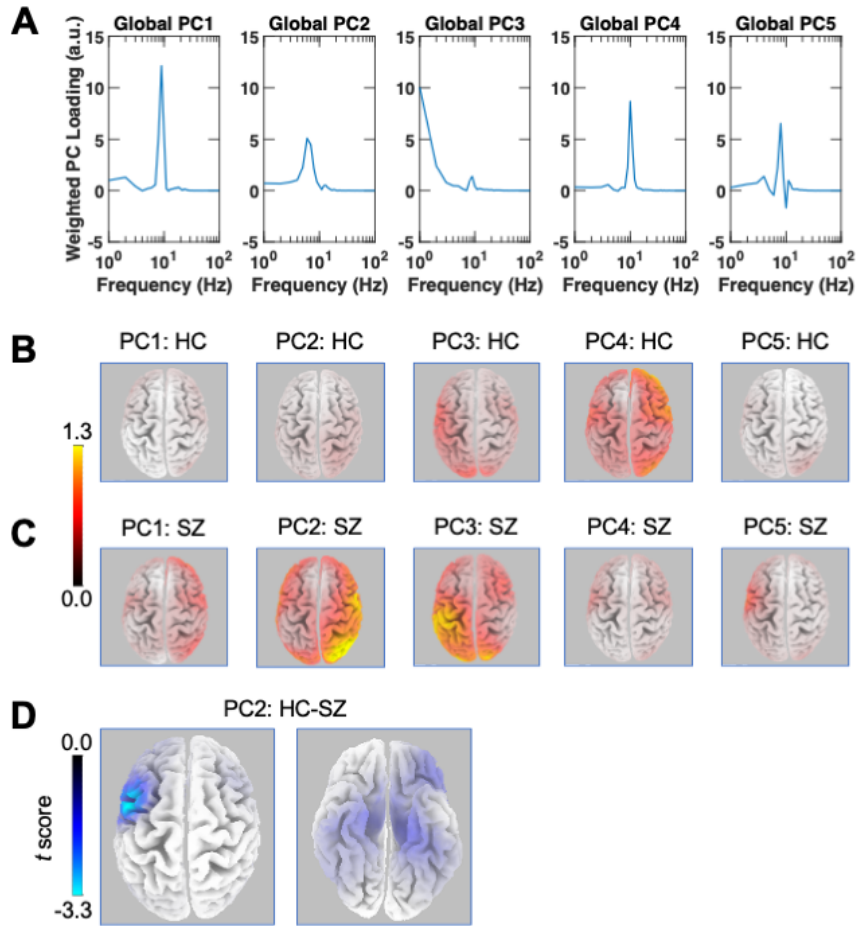


Fig. 4: Source-level PCA results. **(A)** Weighted spectral loadings. PC2 corresponds to the theta/alpha PC3 in the sensor-level global PCA. **(B, C)** PC score distributions for **(B)** HC and **(C)** SZ. Dorsal views of the inflated cortical surface are shown. The color bar indicates PC score values. **(D)** Anatomical distribution of HC minus SZ t scores for PC2. Voxels for which the contrast was significant (following max-stat correction) are colored (range is $-3.3 < t < -2.7$). Dorsal (left) and ventral (right) views of the inflated cortical surface are shown.